J. Fluid Mech. (2016), *vol.* 804, R2, doi:10.1017/jfm.2016.526

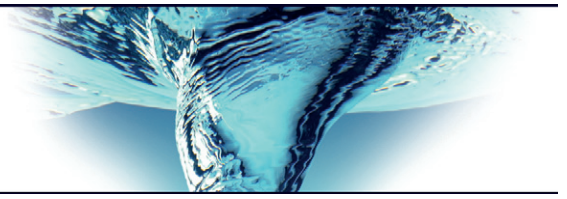

JFM RAPIDS
journals.cambridge.org/rapids

Regeneration of turbulent fluctuations in low-Froude-number flow over a sphere at a Reynolds number of 3700

Anikesh Pal[1], **Sutanu Sarkar**[1,†], **Antonio Posa**[2] **and Elias Balaras**[2]

[1]Department of Mechanical and Aerospace Engineering, University of California San Diego, CA 92093, USA

[2]Department of Mechanical and Aerospace Engineering, The George Washington University, DC 20052, USA

(Received 10 May 2016; revised 27 June 2016; accepted 8 August 2016)

Direct numerical simulations (DNS) are performed to study the behaviour of flow past a sphere in the regime of high stratification (low Froude number Fr). In contrast to previous results at lower Reynolds numbers, which suggest monotone suppression of turbulence with increasing stratification in flow past a sphere, it is found that, below a critical Fr, increasing the stratification induces unsteady vortical motion and turbulent fluctuations in the near wake. The near wake is quantified by computing the energy spectra, the turbulence energy equation, the partition of energy into horizontal and vertical components, and the buoyancy Reynolds number. These diagnostics show that the stabilizing effect of buoyancy changes flow over the sphere to flow around the sphere. This qualitative change in the flow leads to a new regime of unsteady vortex shedding in the horizontal planes and intensified horizontal shear which result in turbulence regeneration.

Key words: stratified turbulence, turbulent flows, wakes/jets

1. Introduction

Wakes of bluff bodies in a density-stratified environment are common, e.g. marine swimmers, underwater submersibles and flows over mountains and around islands. Buoyancy qualitatively changes the far wake, leading to longer lifetime, anisotropic suppression of turbulence and quasi-two-dimensional coherent vortices (Lin & Pao 1979; Spedding 2014). Recent numerical and experimental studies of the benchmark problem of flow past a sphere in a uniformly stratified fluid mostly consider a Froude number $Fr \geqslant O(1)$, where $Fr = U/ND$ is based on the body velocity U, body diameter

† Email address for correspondence: sarkar@ucsd.edu

D and buoyancy frequency N. Strong stratification, e.g. the upper ocean pycnocline, can lead to $Fr \leqslant O(1)$ considered here. Unlike previous low-Fr studies of flow past a sphere, the present Reynolds number of $Re = UD/\nu = 3700$ (ν is the kinematic viscosity) is not small.

The first numerical simulations of the low-Fr case over a sphere (Hanazaki 1988) were at $Re = 200$ (laminar flow). It was found that the flow tends to flow around in the horizontal rather than going over the sphere if $Fr < 0.5$ and eventually approaches two-dimensionality for $Fr < 0.2$. Later experiments (Lin *et al.* 1992; Chomaz, Bonneton & Hopfinger 1993) covered a wide range of Fr and Re, but the low-Fr cases had low Re as well. The near wake was classified into four regimes (Chomaz *et al.* 1993) depending on the Froude number, including the quasi-2D regime which occurred for the lowest examined values of $Fr \in \{0.125, 0.4\}$. A recent direct numerical simulation (DNS) (Orr *et al.* 2015) included $Fr < 1$ cases but at low $Re = 200$. None of these prior studies report turbulence in the low-Fr regime. It has been suggested (Chomaz *et al.* 1993) that the effect of Re is weak when $Fr < 0.35$ as long as Re exceeds 100. On the other hand, quasi-2D motion in strongly stratified flow can be turbulent when the Reynolds number is large, as found for Taylor–Green vortices (Riley & deBruynKops 2003), homogeneous turbulence (Lindborg 2006; Brethouwer *et al.* 2007) and a far wake (Diamessis, Spedding & Domaradzki 2011). The non-equilibrium region of the far wake is also lengthened for large Re (Brucker & Sarkar 2010).

2. Problem formulation, numerical details and validation

Motivated by the unanswered question regarding near-wake turbulence when Fr is low but Re is not, we use DNS to investigate the flow past a sphere at $Re = 3700$ and $Fr \in \{0.025, 1\}$. The three-dimensional Navier–Stokes equations are solved in a cylindrical coordinate system on a staggered grid using an immersed boundary method (IBM) (Balaras 2004; Yang & Balaras 2006) for representing the sphere.

The simulation parameters, domain size and grid distribution for the different cases are given in table 1. High resolution is used at the sphere surface (20 points across the boundary layer thickness at the point of maximum wall shear stress) and in the wake. The radial grid spacing is $\Delta r \simeq 0.0016$ in the cylindrical region ($r < 0.65$) that encloses the sphere, the azimuthal direction has 128 points, and $\Delta x \simeq 0.0016$ near the surface. The grid has mild stretching, radially and streamwise, away from the body. The IBM results and the grid resolution to resolve the flow have been successfully validated in the unstratified case against both previous simulations and laboratory experiments. Figure 1(*a*,*b*) shows that the variations of the surface pressure coefficient, C_p, and the surface shear stress, $(\tau/\rho U^2)Re^{0.5}$ (τ is the shear stress and ρ is the reference density), as a function of the azimuthal angle, match well with results in the available literature. Table 2 shows that key characteristics of the near-body flow such as the Strouhal number (St) of the dominant shedding frequency, the separation angle (φ_s), the coefficient of drag ($\overline{C_d}$) and the pressure coefficient ($\overline{C_{pb}}$) at the rearward stagnation point also match with previously reported values.

3. Results and discussion

Figure 2 shows the downstream evolution of the turbulent kinetic energy (TKE) integrated over cross-stream (x_2–x_3) planes for cases with different Fr. It should be noted that x_3 denotes the vertical coordinate, the horizontal directions are x_1 (streamwise) and x_2 (lateral), and the sphere centre is at the origin. All statistics are

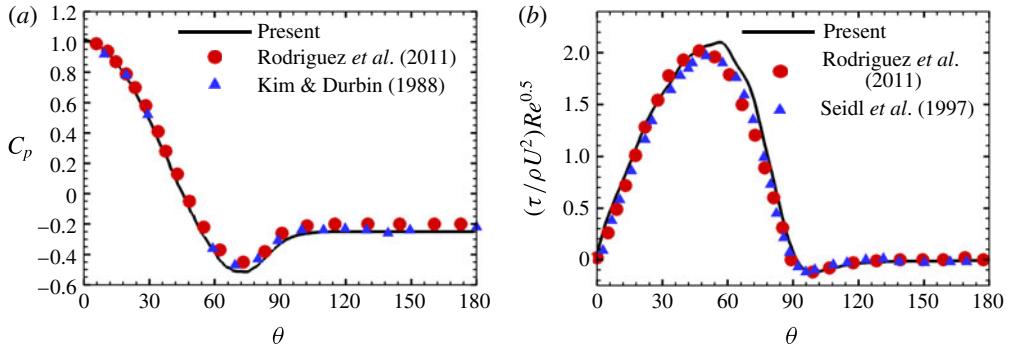

FIGURE 1. Validation of the unstratified wake: (*a*) pressure coefficient, C_p, (*b*) normalized drag coefficient, $(\tau/\rho U^2)Re^{0.5}$. Here, θ is the azimuthal angle, with $\theta = 0$ corresponding to the forward stagnation point.

Case	*Re*	*Fr*	L_r	L_θ	L_z	N_r	N_θ	N_z
1	3700	0.025	58	2π	63 (40 upstream; 23 downstream)	690	128	3072
2	3700	0.05	58	2π	63 (40 upstream; 23 downstream)	690	128	3072
3	3700	0.125	58	2π	120 (40 upstream; 80 downstream)	690	128	4608
4	3700	0.17	58	2π	56 (40 upstream; 16 downstream)	690	128	2560
5	3700	0.21	58	2π	56 (40 upstream; 16 downstream)	690	128	2560
6	3700	0.25	58	2π	120 (40 upstream; 80 downstream)	690	128	4608
7	3700	0.5	58	2π	120 (40 upstream; 80 downstream)	690	128	4608
8	3700	0.8	58	2π	120 (40 upstream; 80 downstream)	690	128	4608
9	3700	1	58	2π	103 (25 upstream; 80 downstream)	690	128	4608
10	3700	∞	16	2π	95 (13 upstream; 80 downstream)	630	128	4608

TABLE 1. Simulation parameters. The sphere is located at (0, 0, 0). The substantial domain size in the radial and upstream directions, along with the sponge region, eliminates the spurious reflection of internal waves.

computed after the initial transient by time averaging over an interval of $1.5L_x/U$ which is sufficient to obtain converged statistics. Buoyancy in a stratified wake has been found to suppress turbulence in previous studies, and, accordingly, the TKE decreases when *Fr* decreases from 1 to 0.8 to 0.5. However, the trend reverses when *Fr* decreases to 0.25 and beyond: the TKE increases with decreasing *Fr*. The value of the TKE in the $Fr = 0.25$ case increases to a level comparable to the $Fr = 0.8$ case, and a further decrease of *Fr* to 0.21 leads to values of the TKE larger than in the unstratified case. Subsequent reduction in *Fr* beyond 0.21 leads to progressive augmentation of the TKE.

To understand the remarkable regeneration of fluctuations in the near wake at low *Fr*, contour plots of the azimuthal vorticity magnitude in the horizontal (x_1–x_2) and vertical (x_1–x_3) planes (figure 3) are examined. The near-wake dynamics changes qualitatively for cases with $Fr \leqslant 0.25$, as elaborated below. The $Fr = 1$ wake displays the anisotropy of a moderate-*Fr* wake: a large spread in the horizontal plane (figure 3*a*) and small-scale structures associated with the shear layer instability, while, in the vertical plane, the separated boundary layers (figure 3*b*) contract, followed by an undulation of the wake. At $Fr = 0.5$ (not shown here), the recirculation bubble

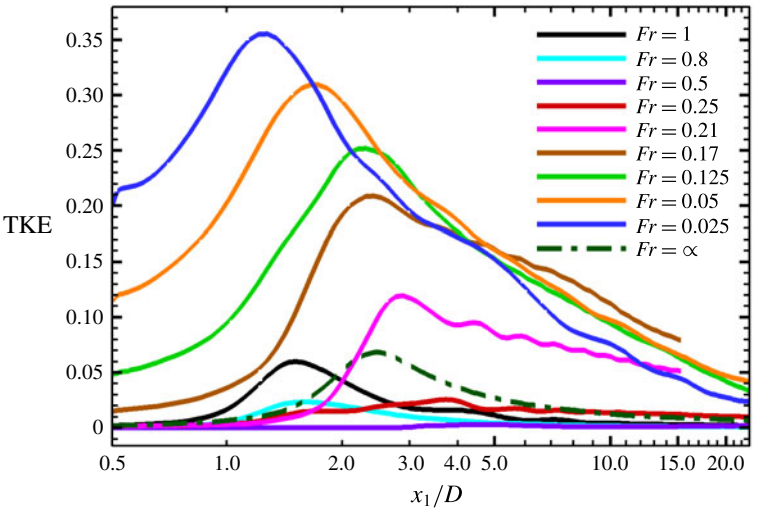

FIGURE 2. Evolution of integrated TKE in the streamwise direction. The plotted quantity is the area-integrated TKE normalized using U and D.

Case	Re	St	φ_s (deg.)	$\overline{C_d}$	$\overline{C_{pb}}$
Present DNS (unstratified case)	3700	0.210	91.7	0.3938	−0.215
Schlichting (1979) (exp.)	3700			0.39	
Kim & Durbin (1988) (exp.)	3700	0.225			−0.224
Sakamoto & Haniu (1990) (exp.)	3700	0.204			
Seidl, Muzaferija & Perić (1997) (DNS)	5000		89.5	0.38	
Tomboulides & Orszag (2000) (DNS)	1000	0.195	102		
Constantinescu & Squires (2003) (LES)	10^4	0.195	85–86	0.393	
Yun, Kim & Choi (2006) (LES)	3700	0.21	90	0.355	−0.194
Rodriguez *et al.* (2011) (DNS)	3700	0.215	89.4	0.394	−0.207

TABLE 2. Comparison of the different statistical flow features of the near-body flow in the present DNS with experimental measurements and numerical results available in the literature. Here, LES stands for large-eddy simulation, $St = fD/U$ is the non-dimensional vortex shedding frequency, φ_s is the azimuthal separation angle, C_d is the drag coefficient and C_{pb} is the rearward pressure coefficient at $\varphi = \pi$.

is steady, the disintegration of the shear layer is suppressed in the horizontal plane and the separating shear layers dip to the centreline in the vertical plane. The shear layer formed by the separating boundary layer exhibits large steady waviness in the vertical plane, there is little unsteadiness in the near wake and, therefore, the TKE for $Fr = 0.5$ is insignificant, as was shown in figure 2. A quasisteady recirculation bubble attached to the sphere is found in the horizontal plane (figure 3*c*) for a larger stratification, $Fr = 0.25$. At the end of the recirculation zone, the wake undergoes an unsteady undulation with the shedding of vortices further downstream. The shear layer in the vertical direction (figure 3*d*) manifests waviness (induced by lee waves), but the instability does not break down into turbulence. The flow between the upper and lower shear layers displays thin strips of enhanced vorticity symptomatic of vorticity layering.

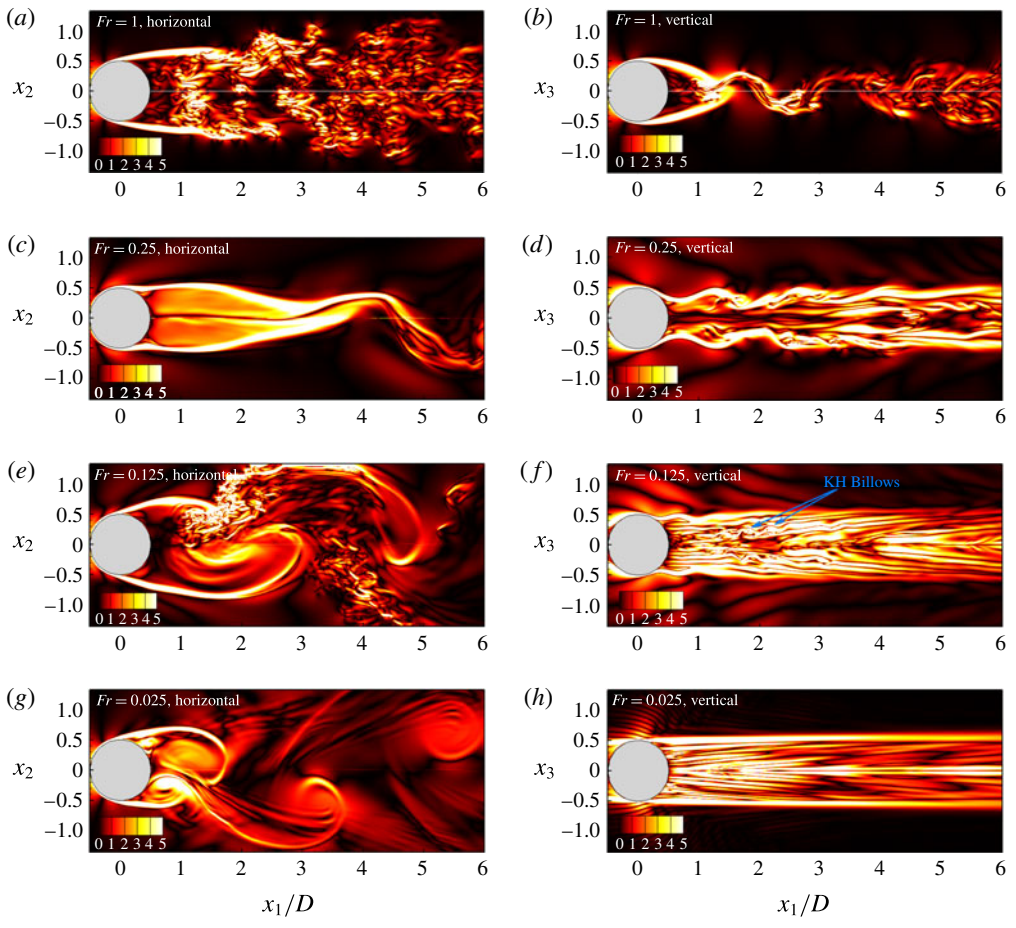

FIGURE 3. Instantaneous azimuthal vorticity magnitude on the horizontal x_1–x_2 centre plane ($x_3 = 0$) and the vertical x_1–x_3 centre plane ($x_2 = 0$). Snapshots compared among cases with different Fr. The plotted vorticity is normalized using U and D.

The flow organization changes significantly with further decrease in Fr to 0.125 and beyond. There is unsteady motion of the shear layers in the horizontal plane accompanied by patches of small-scale turbulence (figure 3*e*) as compared with the steady recirculation bubble in the $Fr = 0.25$ wake. This reappearance of small-scale fluctuations at $Fr = 0.125$ occurs due to unsteady vortex shedding in the horizontal plane, which results in both flapping and destabilization of the shear layer. A similar vertical layering of vorticity to that at $Fr = 0.25$ is also seen at $Fr = 0.125$ but, in this case, the layers roll up intermittently to form Kelvin–Helmholtz (KH) billows (figure 3*f*) which then break down into finer-scale fluctuations. A secondary instability of pancake vortices in the far wake to form KH rolls was noted in previous temporal simulations (Diamessis *et al.* 2011) for sufficiently high Re. In the present near wake, the perturbations provided by the horizontal flapping motion and the value of the local Re are sufficient to destabilize the vertically layered vorticity into KH billows. As Fr approaches 0.025, the unsteady vortex shedding from the sphere in the horizontal plane becomes more noticeable. The TKE in the region $x/D < 1$ which belongs to the very near wake is also the largest among all simulated cases, as was shown in figure 2.

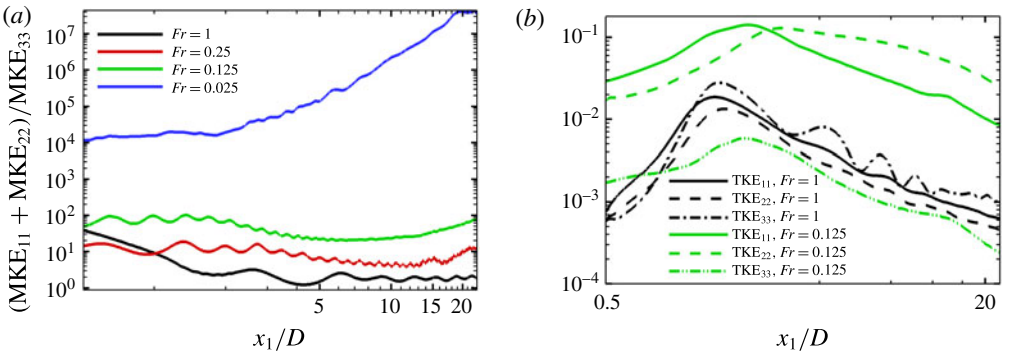

FIGURE 4. Evolution of (*a*) the ratio of area-integrated horizontal and vertical MKEs and (*b*) the components of the integrated TKE, in the streamwise direction. The area integration is over the x_2, x_3 plane normal to the streamwise direction.

In the horizontal plane (figure 3*g*), there are coherent vortices with interspersed threads of rolled-up vorticity. In the vertical plane (figure 3*h*), layered vortical structures are seen but do not manifest KH billows. The fact that KH billows are absent in the $Fr = 0.025$ case will be explained, based on the value of the buoyancy Reynolds number and the scaling analysis of Riley & deBruynKops (2003) and Brethouwer *et al.* (2007), later in the paper. The vorticity pattern at $Fr = 0.025$ appears to have less fine-scale activity relative to $Fr = 0.125$. Internal gravity waves at the body can be seen in the vertical plane (figure 3*d*,*f*,*h*), but their discussion is deferred to future work.

Both the mean and the turbulent kinetic energy are increasingly dominated by horizontal motions as Fr decreases to 0.25 and below. The evolution of the ratio of the area-integrated mean kinetic energies (MKEs) of the horizontal component ($MKE_{11} + MKE_{22}$) and the vertical component (MKE_{33}) is shown in figure 4(*a*). For $Fr = 1$, the horizontal MKE is larger near the sphere, but, beyond $x_1/D \approx 5$, the MKE becomes similarly distributed among the horizontal and vertical components. The undulations after $x_1/D \approx 5$ signify the exchange of MKE between the horizontal and vertical components. The ratio $(MKE_{11} + MKE_{22})/MKE_{33}$ for $Fr = 0.25$ and 0.125 characterizes the transition of the near wake into quasihorizontal motion. The case with $Fr = 0.025$ exhibits the complete dominance of horizontal motion, present primarily in the form of layered coherent vortices that span a wide lateral (x_2) extent. The streamwise variation of the components of the TKE for $Fr = 1$ and 0.125 is presented in figure 4(*b*). The components of the TKE for $Fr = 1$ evolve in a similar manner, whereas for $Fr = 0.25$ (not shown here) the streamwise (TKE_{11}) and spanwise (TKE_{22}) components are larger relative to the vertical (TKE_{33}) component. A significant difference between the horizontal (TKE_{11}, TKE_{22}) and vertical components is observed as Fr is further decreased to 0.125 (shown here) and 0.025 (not shown here).

Temporal spectra are examined to quantify buoyancy effects on the frequency content of the lateral velocity, v. Figure 5(*a*) shows that there is a significant decrease of energy at all frequencies when the stratification increases to change Fr from 1 to 0.25. However, a further decrease of Fr to 0.125 and 0.025 shows a re-energization of fluctuations at all frequencies. There is a strong low-frequency peak in these cases: (i) $St = \omega D/U = 0.163$ for $Fr = 0.125$, (ii) $St = 0.200$ for $Fr = 0.025$. Secondary

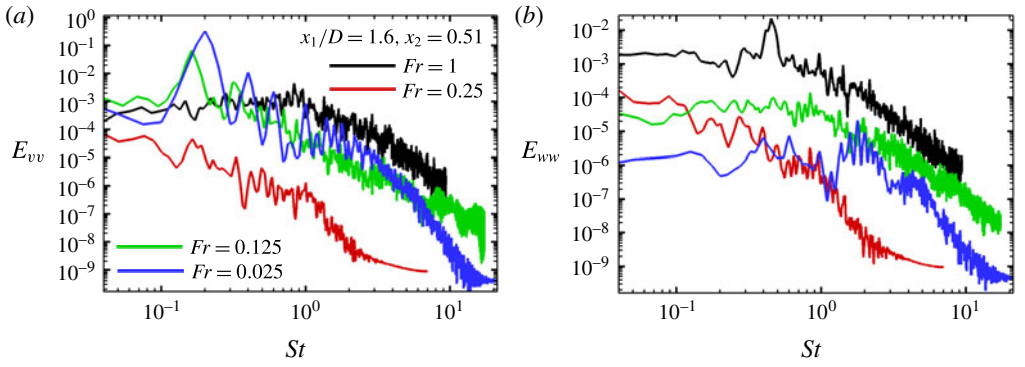

FIGURE 5. Energy spectra of (a) lateral v fluctuations and (b) vertical w fluctuations at a downstream point ($x_1 = 1.6, x_2 = 0.51, x_3 = 0$) in the horizontal centre plane at various Froude numbers. Here, E_{vv}, E_{ww} and the Strouhal number, St, are non-dimensional values based on U and D.

peaks of E_{vv} at harmonics of the low-frequency mode are also evident. There is substantial energy, much larger than at $Fr = 0.25$, at the intermediate frequencies as well. It should be noticed that for flow over a circular cylinder in an unstratified environment at $Re = 3900$, the shedding frequency is found to be ≈ 0.2 (Parnaudeau *et al.* 2008). Therefore, with increasing stratification, the vortex shedding of a sphere shifts towards that of a circular cylinder. This is because the flow at depths larger than $O(U/N)$ with respect to the top of the sphere tends to divert around the sphere rather than over the sphere because of the potential energy barrier. We emphasize that the low-Fr near wake, apart from the similarity of vortex shedding, is quite different from the unstratified cylinder wake, where the strong inhibition of vertical fluctuations by buoyancy is absent. For example, the vertical velocity spectra E_{ww} (figure 5*b*) at $Fr = 0.125$ and $Fr = 0.025$ have much smaller amplitudes relative to their corresponding horizontal counterparts, E_{vv}, and also have smaller amplitudes with respect to E_{ww} for the $Fr = 1$ case.

The mean velocity profiles change significantly with decreasing Fr because of the preferential flow around the sphere rather than over it. Thus, the profile of the mean streamwise velocity (figure 6*a*) along the lateral line ($x_1 = x_3 = 0, x_2 > 0.5$) shows enhanced horizontal shear in the vicinity of the sphere boundary at $x_2 = 0.5$ for the lower-Fr cases in comparison with $Fr = 1$. At $x_1 = 1$ (figure 6*b*), the shear is confined within a narrow band of $0.5 < x_2 < 0.8$ for $Fr = 1$, whereas $Fr = 0.25$, 0.125 and 0.025 show progressively broader regions of shear. The lateral horizontal motion of the fluid near the sphere is also enhanced, as shown by the profile of the lateral velocity $U_{2,mean}(x_2)$ on the line ($x_1 = x_3 = 0, x_2 > 0.5$) in figure 6(*c*). At $x_1 = 1$, the variation of $U_{2,mean}$ as a function of x_2 (figure 6*d*) is substantial for $Fr = 0.25$, 0.125 and 0.025 and has a complex shape because of the three-dimensional mean flow near the body.

The production of TKE is given by $P = -\overline{u_i' u_j'} \partial \bar{U}_i / \partial x_j$, with the overbar denoting a mean value. The various components $P_{\alpha,\beta}$ that comprise P change in the near wake ($x/D < 5$) because of the buoyancy effect. Figure 7 shows the downstream evolution of the components $P_{\alpha,\beta}$ integrated over the cross-stream x_2–x_3 plane. The integrated production for the $Fr = 1$ wake is primarily dominated by the components (P_{13}, P_{31}) involving vertical fluctuations u_3', with some contributions from the components (P_{12}, P_{22}) involving horizontal fluctuations u_2', as shown in figure 7(*a*). This scenario

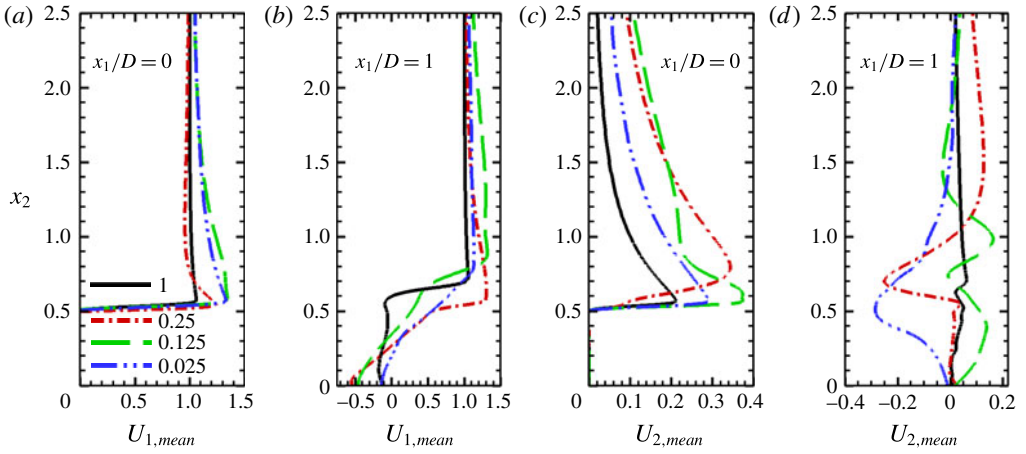

FIGURE 6. Streamwise ($U_{1,mean}$) and lateral ($U_{2,mean}$) mean velocity profiles are plotted as a function of the lateral coordinate x_2 at two streamwise locations ($x_1/D = 0, 1$) in the horizontal central plane, $x_3 = 0$. The plotted velocity has been normalized with U and the x_2 coordinate with D.

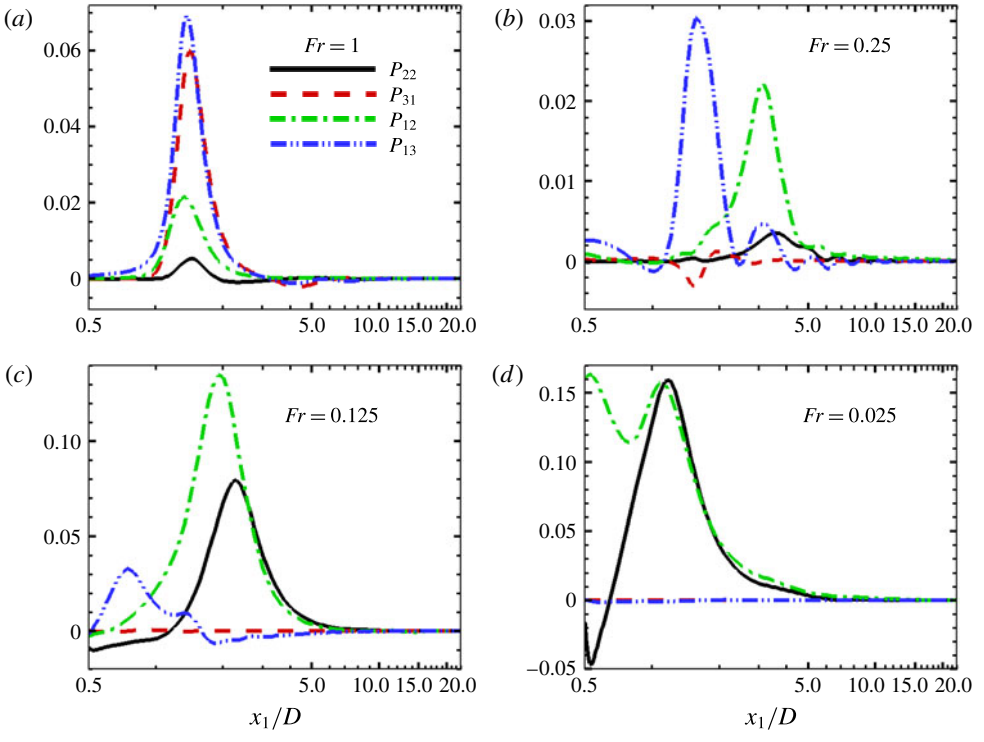

FIGURE 7. Shear production components for different Fr cases, integrated over x_2–x_3 planes. The plotted production components have been normalized with U and D.

changes when the stratification increases. As illustrated in figure 7(*b*) for $Fr = 0.25$, the components P_{13} and especially P_{31} are suppressed with respect to $Fr = 1$, and by $Fr = 0.025$ (figure 7*d*), both become negligible as the buoyancy effect strengthens

to make u_3' negligible. However, P_{12} and P_{22} associated with horizontal fluctuations increase when Fr is reduced to 0.125 from 0.25. The large lateral (x_2) gradients of mean U_1 (figure 6*b*) and mean U_2 (figure 6*d*) enhance P_{12} and P_{22} respectively, making them the leading production terms for $Fr = 0.125$ and 0.025.

The buoyancy Reynolds number, $Re_b = \varepsilon/\nu N^2$, where ε is the turbulent dissipation rate and N is the background buoyancy frequency, is an often-used parameter to distinguish the turbulent nature of fluctuations in stratified flow. A similar parameter that distinguishes turbulence is $\mathscr{R} = ReFr_h^2$, where $Fr_h = u/l_hN$ (l_h is the length scale and u is the velocity scale of horizontal fluctuations) is the horizontal Froude number and $Re = ul_h/\nu$. The choice of $l_h = u^3/\varepsilon$ makes $\mathscr{R}$ identical to Re_b. Riley & deBruynKops (2003) estimated the Richardson number of layered motions in strongly stratified flow by $Ri \simeq 1/\mathscr{R}$, and proposed that layer instability was possible if $Ri \lesssim 1$ or, equivalently, $\mathscr{R} \gtrsim 1$. Brethouwer *et al.* (2007) concluded that if $\mathscr{R} \gg 1$, an energy cascade from large to small scales is possible, allowing an inertial range in horizontal energy spectra. In contrast, for $\mathscr{R} \ll 1$, the dissipation ε is associated with quasi-two-dimensional scales. Arobone & Sarkar (2010), in their DNS of a stratified fluid with horizontal shear, found a network of quasi-2D vortices with interspersed dislocations that were laminar for small Re_b but exhibited secondary instability for larger Re_b.

We find that the values of Re_b (figure 8) provide guidance to the observed differences in the state of fluctuating motion at different Fr. The $Fr = 1$ case has Re_b values between 10–100 at $0.54 < x_1/D < 5.5$, signifying broadband turbulence, as observed from the energy content at high frequencies in the horizontal and vertical energy spectra (figure 5*a*,*b*). For the lower Fr of 0.25, the streamwise locations $0.5 < x_1/D < 3$ have $0.1 < Re_b < 1$. At these streamwise locations, the vortices are still attached, as shown in figure 3(*c*), and no small-scale features are present. Some of the small scales observed in the $Fr = 0.25$ case (figure 3*c*) at $x_1/D = 4$–5 are consistent with $Re_b \gtrsim 1$ in this region. The small scales observed in figure 3(*e*) are consistent with the $O(1)$ values of Re_b for $Fr = 0.125$ at locations $1.14 < x_1/D < 2.75$, where $Re_b < 1$ and the flow transitions towards quasi-2D dissipation. For $Fr = 0.025$, $Re_b \ll 1$ at all x_1/D locations. There is vertical shear between pancake eddies, as shown in figure 3(*f*,*h*), which is quasi-laminar for small Re_b, consistent with Brethouwer *et al.* (2007). Nevertheless, the flow is far from laminar. The horizontal motion is unsteady due to vortex shedding, there is broadband turbulence in the near wake, as shown by velocity spectra, and there are small scales, e.g. thin braid vortices between the vortices being shed from the sphere (figure 3*g*) in the vorticity field.

From figure 8, it can be seen that for $Fr = 0.25$ and 0.125, the value of $Ri \approx 1/Re_b$ is $\lesssim 1$ and, therefore, secondary KH instabilities are present in the vertical layers (figure 3*d*,*f*). However, for $Fr = 0.125$ at $x_1/D > 5$, the value of $Ri > 1$, and for $Fr = 0.025$, the value of $Ri \gg 1$ at all x_1/D locations. Hence, secondary instability is absent in the vertical layers at the $x_1/D \approx 5$ location in figure 3(*f*) and at all locations in figure 3(*h*).

4. Conclusions

To summarize, although turbulence decreases and is almost extinguished when stratification increases and Fr decreases to 0.5, it is regenerated when Fr decreases further to 0.25 and beyond at $Re = 3700$. This new finding is contrary to the belief that turbulence suppression is monotone with increasing stratification for flow past a sphere, which was based on experiments at low Re. Owing to the suppression

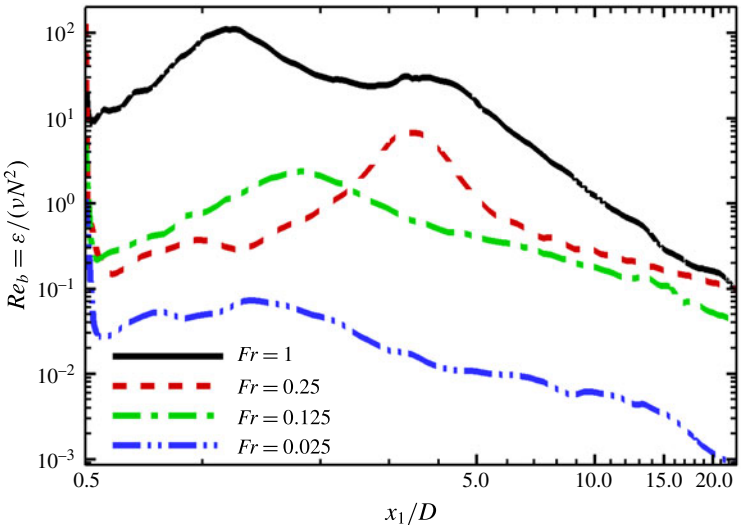

FIGURE 8. Variation of the buoyancy Reynolds number $Re_b = \varepsilon/(\nu N^2)$ for different Fr at the centre line $x_2 = 0, x_3 = 0$ in the streamwise direction x_1.

of vertical motion, the fluid moves horizontally around the sphere. This leads to a new regime of unsteady vortex shedding with frequency similar to that for a circular cylinder, there is a transition to broadband turbulence if Re is sufficiently large, and the enhanced shear of the horizontal motion feeds energy into the fluctuation energy. The buoyancy Reynolds number is $Re_b = O(1)$ at locations in the low-Fr wake where quasi-2D vortices are accompanied by small-scale features in vertical layers between these vortices. Future simulations of flow past a sphere at higher Re are desirable to explore the low-Fr dynamics of the near wake at higher Re_b.

Acknowledgements

We gratefully acknowledge the support of ONR grant no. N00014-15-1-2718 administered by Dr R. Joslin. Computational resources were provided by the Department of Defense High Performance Computing Modernization Program.

References

AROBONE, E. & SARKAR, S. 2010 The statistical evolution of a stratified mixing layer with horizontal shear invoking feature extraction. *Phys. Fluids* **22**, 1–15.

BALARAS, E. 2004 Modeling complex boundaries using an external force field on fixed Cartesian grids in large-eddy simulations. *Comput. Fluids* **33** (3), 375–404.

BRETHOUWER, G., BILLANT, P., LINDBORG, E. & CHOMAZ, J. M. 2007 Scaling analysis and simulation of strongly stratified turbulent flows. *J. Fluid Mech.* **585**, 343–368.

BRUCKER, K. A. & SARKAR, S. 2010 A comparative study of self-propelled and towed wakes in a stratified fluid. *J. Fluid Mech.* **652**, 373–404.

CHOMAZ, J. M., BONNETON, P. & HOPFINGER, E. J. 1993 The structure of the near wake of a sphere moving horizontally in a stratified fluid. *J. Fluid Mech.* **254**, 1–21.

CONSTANTINESCU, G. S. & SQUIRES, K. D. 2003 LES and DES investigations of turbulent flow over a sphere at $Re = 10\,000$. *FTC* **70** (1–4), 267–298.

DIAMESSIS, P. J., SPEDDING, G. R. & DOMARADZKI, J. A. 2011 Similarity scaling and vorticity structure in high Reynolds number stably stratified turbulent wakes. *J. Fluid Mech.* **671**, 52–95.

HANAZAKI, H. 1988 A numerical study of three-dimensional stratified flow past a sphere. *J. Fluid Mech.* **192**, 393–419.

KIM, H. J. & DURBIN, P. A. 1988 Observations of the frequencies in a sphere wake and of drag increase by acoustic excitation. *Phys. Fluids* **31** (11), 3260–3265.

LIN, J. T. & PAO, Y. H. 1979 Wakes in stratified fluids. *Annu. Rev. Fluid Mech.* **11**, 317–338.

LIN, Q., LINDBERG, W. R., BOYER, D. L. & FERNANDO, H. J. S. 1992 Stratified flow past a sphere. *J. Fluid Mech.* **240**, 315–354.

LINDBORG, E. 2006 The energy cascade in a strongly stratified fluid. *J. Fluid Mech.* **550**, 207–242.

ORR, T. S, DOMARADZKI, J. A., SPEDDING, G. R. & CONSTANTINESCU, G. S. 2015 Numerical simulations of the near wake of a sphere moving in a steady, horizontal motion through a linearly stratified fluid at $Re = 1000$. *Phys. Fluids* **27** (3), 035113.

PARNAUDEAU, P., CARLIER, J., HEITZ, D. & LAMBALLAIS, E. 2008 Experimental and numerical studies of the flow over a circular cylinder at Reynolds number 3900. *Phys. Fluids* **20** (8), 085101.

RILEY, J. J. & DEBRUYNKOPS, S. M. 2003 Dynamics of turbulence strongly influenced by buoyancy. *Phys. Fluids* **15** (7), 2047–2059.

RODRIGUEZ, I., BORELL, R., LEHMKUHL, O., PEREZ SEGARRA, C. D. & OLIVA, A. 2011 Direct numerical simulation of the flow over a sphere at $Re = 3700$. *J. Fluid Mech.* **679**, 263–287.

SAKAMOTO, H. & HANIU, H. 1990 A study on vortex shedding from spheres in a uniform flow. *Trans. ASME J. Fluids Engng* **112** (4), 386–392.

SCHLICHTING, H. 1979 *Boundary Layer Theory*, 7th edn. McGraw-Hill.

SEIDL, V., MUZAFERIJA, S. & PERIĆ, M. 1997 Parallel DNS with local grid refinement. *Appl. Sci. Res.* **59** (4), 379–394.

SPEDDING, G. R. 2014 Wake signature detection. *Annu. Rev. Fluid Mech.* **46**, 273–302.

TOMBOULIDES, A. G. & ORSZAG, S. A. 2000 Numerical investigation of transitional and weak turbulent flow past a sphere. *J. Fluid Mech.* **416**, 45–73.

YANG, J. & BALARAS, E. 2006 An embedded-boundary formulation for large-eddy simulation of turbulent flows interacting with moving boundaries. *J. Comput. Phys.* **215** (1), 12–40.

YUN, G., KIM, D. & CHOI, H. 2006 Vortical structures behind a sphere at subcritical Reynolds numbers. *Phys. Fluids* **18** (1), 105102.